Carbon solute drag effect on the growth of carbon supersaturated bainitic ferrite Modeling and experimental validations

Dai, Zongbiao; Chen, Hao; Sun, Junjie; van der Zwaag, Sybrand; Sun, Jun

DOI
10.1016/j.actamat.2024.119791

Publication date
2024

Document Version
Final published version

Published in
Acta Materialia

Acta Materialia 268 (2024) 119791

Contents lists available at ScienceDirect

Acta Materialia

journal homepage: www.elsevier.com/locate/actamat

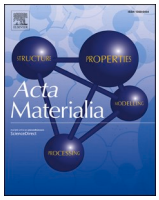

Carbon solute drag effect on the growth of carbon supersaturated bainitic ferrite: Modeling and experimental validations

Zongbiao Dai [*,a], Hao Chen [b], Junjie Sun [a], Sybrand van der Zwaag [c], Jun Sun [a,*]

[a] State Key Laboratory for Mechanical Behavior of Materials, Xi'an Jiaotong University, Xi'an, China
[b] Key Laboratory for Advanced Materials of Ministry of Education, School of Materials Science and Engineering, Tsinghua University, Beijing, China
[c] Faculty of Aerospace Engineering, Delft University of Technology, Kluyverweg 1, Delft, 2629 HS, the Netherlands

ARTICLE INFO

Keywords:
Bainite formation
Carbon diffusion
Carbon supersaturation
Energy dissipation
Lengthening kinetics

ABSTRACT

The carbon partitioning and lengthening rate of bainitic ferrite (α_b) are excellent experimental parameters to estimate our level of understanding of the mechanism of bainitic transformation from a continuum perspective and our ability to capture it in analytical expressions. For Fe-C alloys and relatively simple steels the classical Zener-Hillert theory captures the bainitic transformation rather well but mispredicts the level of carbon in solution in the bainite and overestimates the lengthening rates for transformations at lower temperatures. To address this issue, this paper presents a new thermo-kinetic model based on the Zener-Hillert theory and the Gibbs energy balance concept to simulate the lengthening behavior of α_b in the Fe-C and low alloyed steels. The model incorporates the effect of the temperature dependent carbon diffusion within the migrating interface via a temperature dependent ferrite/austenite interfacial energy and a temperature dependent diffusion coefficient but does not impose local equilibrium across the interface. The good agreement between the model predictions and nine sets of published experiments indicates that both the carbon supersaturation in α_b and the slower lengthening rate are caused by carbon diffusion within the migrating interface. It is found that the degree of carbon supersaturation in α_b increases significantly with decreasing temperature. Consequently, the enhanced carbon solute drag effect, resulting from carbon diffusion within the interface, strongly retards the lengthening rates of α_b at lower temperatures. Transformation strain is shown to have a modest effect on the lengthening rates but to lower the degree of carbon supersaturation.

1. Introduction

Bainitic steels whose production relies primarily on the use of the bainitic transformation to create excellent mechanical properties are being used extensively in automotive, railway and aerospace industries [1,2]. While the relevance of bainitic steels is undisputed, fine details of the bainitic transformation have been a subject of controversy in the physical metallurgy community [2–5]. Until now, there are two competing perspectives regarding the growth mechanism of bainitic ferrite (α_b), known as the diffusionless view and the diffusional view. The former suggests that α_b grows in a diffusionless way and that carbon redistributes or precipitates as carbides after the formation of carbon supersaturated α_b [1,6,7]. The latter assumes that carbon must escape from α_b during the formation of α_b and that the growth kinetics of α_b is controlled by carbon diffusion in austenite (γ) [8–12].

Examination of the carbon partitioning behavior between α_b and γ as a function of transformation temperature and steel composition is one of the main options to analyze the key features in the transformation, and from this to clarify, the mechanism of the bainitic transformation. Various advanced experimental technologies, e.g. field-emission electron probe microanalysis (FE-EPMA) [13,14], atom probe tomography (APT) [15–23], high energy X ray diffraction (HE-XRD) [22,24] and electron energy loss spectroscopy (EELS) [22], have been used to analyze the carbon redistribution in bainite. FE-EPMA [13,14] and APT [15,16] experiments showed that the carbon level in solution for bainite formed at high transformation temperatures (>~450℃) is quite comparable with the paraequilibrium (PE) value. However, extensive APT [17–23] and HE-XRD [22,24] experiments showed conclusively that the carbon content in α_b formed at low transformation temperatures (<~450℃) is much higher than the paraequilibrium value, which is called the 'carbon supersaturation in α_b' phenomenon. Recently, using a unique combination of APT, HE-XRD and EELS, Pushkareva et al. [22]

* Corresponding authors.
E-mail addresses: dzb2022@mail.xjtu.edu.cn (Z. Dai), junsun@mail.xjtu.edu.cn (J. Sun).

https://doi.org/10.1016/j.actamat.2024.119791
Received 21 September 2023; Received in revised form 10 January 2024; Accepted 22 February 2024
Available online 23 February 2024

further proved that a considerable amount of carbon remains trapped in α_b up to 430℃ in low carbon carbide-free bainitic steels. In summary, it has been experimentally established that the degree of carbon supersaturation in α_b strongly depends on temperature and composition [17,19,20,23].

The growth kinetics of α_b is another critical feature to analyze the bainitic transformation. According to the diffusional mechanism, carbon partitioning behavior strongly interacts with the growth kinetics of α_b, which can be described using the classical Zener-Hillert (Z-H) theory [25–27]. For lack of a better insight, the Z-H theory assumes that carbon is in local equilibrium at the migrating interface, i.e. absence of carbon supersaturation in α_b. The constant lengthening rate predicted by the Z-H theory is indeed consistent with various ex-situ [28,29] and in-situ [30–34] experiments. However, the measured lengthening rate is usually slower than that predicted by the Z-H theory [29,35–38] and the discrepancies between them become larger with decreasing temperature and/or enhancing bulk carbon content [37,39]. Kaufman et al. [36] proposed that these differences are attributed to the uncertainty of the bainitic ferrite/austenite (α/γ) interfacial energy used in the Z-H theory. Instead of evaluating the interfacial energy, Leach et al. [37,40] suggested to reconcile these differences via adding a temperature- and composition-dependent 'energy barrier' to the migrating interface. Recently, Benrabah et al. [12] suggested that the energy barrier arises from the interaction between the disconnections at the α /γ interface and the defects in γ matrix such as dislocations and solute atoms. However, in the above studies, the existence of a carbon supersaturated α_b has not been considered when predicting the lengthening behavior of α_b.

The phenomenon of carbon supersaturation in α_b indicates that carbon deviates significantly from local equilibrium at the migrating interface, which is inconsistent with the assumption in the Z-H theory. It has been well established that, due to the deviation from local equilibrium, the trans-interface diffusion of solute atoms would lead to an energy dissipation and thus retard the kinetics of interface migration [41,42]. This is similar to the solute drag effect on the grain boundary migration, thus the Gibbs energy dissipated by trans-interface diffusion is also referred to as solute drag [41–43]. Taking the trans-interface diffusion of carbon into account, Hillert [25,42] and Ågren [44] analyzed the growth behavior of plate-like α in the Fe-C steels using a sharp-interface model, i.e. the so-called Hillert–Ågren model [41]. They predicted that the spontaneous transition from diffusional to diffusionless transformation could occur with decreasing bulk carbon content, which indicates that the presence of carbon supersaturated α_b is possible for the diffusional bainitic transformation. Later, thick-interface models based on the Hillert-Ågren model were developed to carefully consider the diffusion of carbon [45], as well as its co-segregation with substitutional alloying elements [46,47], inside the migrating interface. Using these thick-interface models, Liu further predicted that α is supersaturated with carbon below certain temperatures for the Fe-C systems [45], and found that carbon diffusion plays a dominant role in the lengthening behavior of α_b in the Fe-C-Mo alloys [47]. However, until now, the temperature/composition conditions under which the phenomenon of carbon supersaturation in α_b occurs and its influence on the lengthening kinetics of α_b have not yet been quantitatively clarified.

In this contribution, we aim to find out the physical origin of carbon supersaturation in α_b, and emphasize the critical role of carbon solute drag in the growth behavior of α_b. Therefore, a thermo-kinetic model based on the Z-H theory and the Gibbs energy balance (GEB) concept was proposed to simulate the lengthening behavior of α_b in a series of Fe-C and low-alloyed steels, and using data from nine publications to validate the model. The influences of temperature and composition on the lengthening rate and carbon supersaturation in α_b were systematically investigated, and the model was also used to estimate the effect of transformation strain.

2. Evaluated experimental data from literature

Table 1 shows the chemical compositions, transformation temperatures and the relevant experimental methods of acquiring data for the nine investigated steels as well as the publications from which the data were obtained. The experimental data for three Fe-C alloys, which are denoted as MC, HC-1 and HC-2 respectively, allowed us to study the lengthening kinetics of α_b over quite a wide range of bulk carbon contents and transformation temperatures. In these Fe-C alloys, carbide formation, which will affect both lengthening rate and the level of carbon in solid solution, can not be excluded. To avoid the interference of carbide precipitation, the lengthening kinetics of α_b in two medium carbon low alloyed steels containing 1.5∼2.0 wt.% Si, denoted as MC-HSi-1 and MC-HSi-2 respectively, were also added to the model validation data sets. The level of carbon in solid solution in α_b for four low alloyed steels, which are denoted as MC-LSi, MC-HSi-3, HC-HSi-1 and HC-HSi-2, respectively, were measured using APT and these data also formed part of the validation data sets. In the data screening of these publications values related to carbon-enriched regions due to carbides precipitation, carbon segregation at dislocations and boundaries were excluded. In this study, the lengthening rate and carbon content in α_b for all steels were calculated for temperatures between the bainite start temperature and the martensite start temperature [48]. Calculations were preformed both for the new model and the classical Z-H model and the results were compared with the experimental data.

3. Models

3.1. Carbon diffusion controlled lengthening behavior

The lengthening process of a α_b in an infinite γ matrix was considered using a topology as shown in Fig. 1a. Assuming that there is no diffusion of carbon in α_b matrix after its formation, the lengthening rate v controlled by carbon diffusion ahead of the α/γ interface can be calculated from the Z-H equation [49]:

$$v = \frac{D_C^\gamma}{L}\frac{x_C^{\gamma/\alpha} - x_C^M}{x_C^M - x_C^\alpha} \tag{1}$$

where D_C^γ is the diffusion coefficient of carbon in γ, L is the effective diffusion distance of carbon in γ, x_C^M is the mole fraction of carbon in the matrix, x_C^α and $x_C^{\gamma/\alpha}$ are the mole fractions of carbon at the interface in α_b and γ, respectively. Since D_C^γ is very sensitive to carbon content [50] and a sharp carbon content gradient develops ahead of the interface in γ, an effective diffusion coefficient as suggested by Trivedi and Pound [51] was adopted into Eq. (1):

$$D_{C;\mathrm{eff}}^\gamma = \frac{1}{x_C^{\gamma/\alpha} - x_C^L}\int_{x_C^L}^{x_C^{\gamma/\alpha}} D_C^\gamma(x_C)dx_C \tag{2}$$

where x_C^L is the mole fraction of carbon at the diffusion distance L from the α/γ interface. x_C^L is chosen to be x_C^M. L is usually assumed to be proportional to the curvature radius r of the growing α_b, i.e. $L = 2r$ [49].

Taking the capillarity effect into account, the dissipation of Gibbs energy due to the curvature is given by:

$$\Delta G_m^{curv} = P_1 V_m = \frac{\sigma^{\alpha/\gamma}}{r} V_m \tag{3}$$

where P_1 is the pressure due to the interfacial energy, V_m is the molar volume and $\sigma^{\alpha/\gamma}$ is the interfacial energy. Inserting Eq. (2) and (3) in Eq. (1), one obtains:

$$v = \frac{D_{C;\mathrm{eff}}^\gamma}{2\sigma^{\alpha/\gamma}}\frac{\Delta G_m^{curv}}{V_m}\frac{x_C^{\gamma/\alpha} - x_C^M}{x_C^M - x_C^\alpha} \tag{4}$$

Table 1
Chemical compositions, bainitic transformation temperatures and the relevant experimental methods of acquiring data for the investigated steels.
HC: high carbon; MC: medium carbon; HSi: high silicon; LSi: low silicon.
OM: optical microscope; TEM: transmission electron microscope; CLSM: confocal laser scanning microscope; APT: atom probe tomography.

Steels	Chemical compositions (wt.%)	Temperatures (K)	Experimental methods of acquiring data		Refs.
			Lengthening rate	C content in α_b	
MC	Fe-0.33C	723~973	Ex-situ OM	×	[28]
HC-1	Fe-0.91C	543~673	In-situ OM	×	[31]
HC-2	Fe-1.43C	456~538	In-situ OM	×	[30]
MC-HSi-1	Fe-0.3C-3.0Mn-1.5Si-0.15Mo	573; 643~653	In-situ TEM	×	[34]
MC-HSi-2	Fe-0.4C-2.8Mn-2.0Si	573; 606~649; 671~682; 676~696	In-situ CLSM	×	[32]
MC-LSi	Fe-0.30C-1.22Mn-0.25Si-0.14Cr-0.03Mo-0.10Ni	648; 673; 698; 748; 773; 798	×	APT	[17,18]
MC-HSi-3	Fe-0.29C-2.06Mn-1.48Si-0.43Cr-0.27Mo	598; 623; 648; 698	×	APT	[17,18]
HC-HSi-1	Fe-0.70C-1.30Mn-1.40Si-1.0Cr-0.24Mo-0.1Ni	493; 523	×	APT	[17,18]
HC-HSi-2	Fe-0.98C-1.89Mn-1.46Si-1.26Cr-0.26Mo-0.09V	473; 573	×	APT	[17,18]

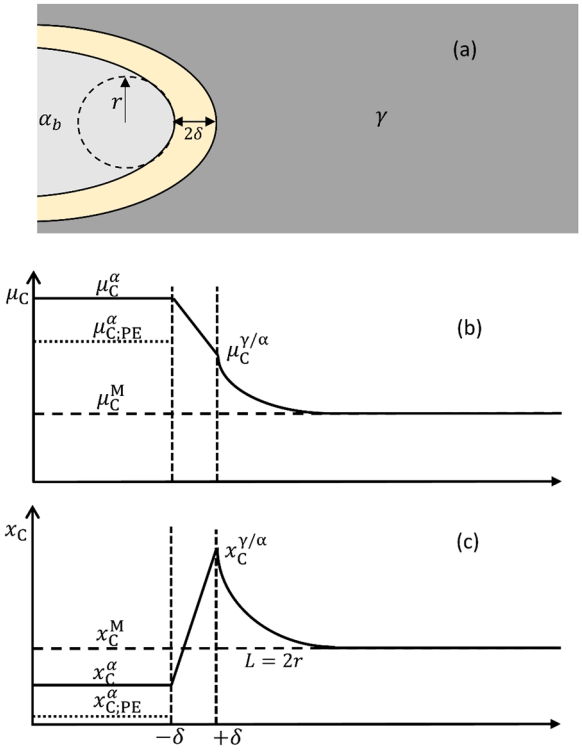

Fig. 1. Schematic illustrations of (a) the growth of a plate-like bainitic ferrite in an infinite austenite matrix, (b) chemical potential of carbon and (c) carbon profile across the interface. PE: paraequilibrium.

In the above Z-H model, it is usually assumed that carbon is in local equilibrium across the migrating interface. In principle, the deviation from local equilibrium for carbon could occur, especially at low temperatures. Therefore, the diffusion of carbon within the migrating interface should be considered too. Under the assumption of quasi-steady state, the diffusion of carbon inside the migrating interface can be described by [52]:

$$\frac{\partial}{\partial z}\left[D_C^{Intf}\frac{\partial x_C}{\partial z}+\frac{D_C^{Intf}x_C}{RT}\frac{\partial \mu}{\partial z}+vx_C\right]=0 \tag{5}$$

where R is the gas constant, T is the absolute temperature, z is the distance and D_C^{Intf} is the diffusion coefficient of carbon inside the α /γ interface. For the sake of simplicity, the interaction between carbon atoms and the interface was neglected. Therefore, as shown in Fig. 1b, the chemical potential of carbon can be assumed to change linearly inside the α/γ interface:

$$\mu_C=\frac{\mu_C^{\gamma/\alpha}+\mu_C^{\alpha}}{2}+\frac{\mu_C^{\gamma/\alpha}-\mu_C^{\alpha}}{2\delta}z \tag{6}$$

where δ is the half width of the α/γ interface, $\mu_C^{\gamma/\alpha}$ and μ_C^{α} are the chemical potentials of carbon at the interface in γ and α_b, respectively, and z is the position within the interface scaled to the half width. Under such a condition, the simplest solution for Eq. (5) is given by:

$$x_C=\frac{x_C^{\gamma/\alpha}+x_C^{\alpha}}{2}+\frac{x_C^{\gamma/\alpha}-x_C^{\alpha}}{2\delta}z \tag{7}$$

when

$$v=-\frac{D_C^{Intf}}{RT}\frac{\partial \mu}{\partial z}=\frac{D_C^{Intf}}{RT}\frac{\mu_C^{\alpha}-\mu_C^{\gamma/\alpha}}{2\delta} \tag{8}$$

As shown in Eq. (7) and Fig. 1c, the obtained carbon profile changes linearly inside the α/γ interface, which is identical to the assumption by Liu [45]. It is also worth mentioning that Eq. (8) is equal to that obtained via thermodynamic extremal principle (TEP) method by Gamsjäger and Rettenmayr [53].

The dissipation of Gibbs energy due to the carbon diffusion inside the migrating interface ΔG_m^{diff} can be expressed as [43]:

$$\Delta G_m^{diff}=P_2V_m=-\int_{-\delta}^{+\delta}\left(x_C-x_C^{\alpha}\right)\frac{\partial \mu}{\partial z}dz \tag{9}$$

where P_2 is the solute drag force. Inserting Eqs. (6) and (7) into Eq. (9), one obtains:

$$\Delta G_m^{diff}=\frac{1}{2}\left(x_C^{\gamma/\alpha}-x_C^{\alpha}\right)\left(\mu_C^{\alpha}-\mu_C^{\gamma/\alpha}\right) \tag{10}$$

By combining Eqs. (8) and (10), it yields

$$v=\frac{D_C^{Intf}}{\delta RT}\frac{\Delta G_m^{diff}}{x_C^{\gamma/\alpha}-x_C^{\alpha}} \tag{11}$$

According to the interfacial Gibbs energy balance concept, the chemical driving force ΔG_m^{chem} at the migrating interface should be balanced with the total dissipation of Gibbs energy $\Delta G_m^{total-diss}$ due to various factors, i.e.:

$$\Delta G_m^{chem}=\Delta G_m^{curv}+\Delta G_m^{diff}+\Delta G_m^{fric}+\Delta G_m^{strain} \tag{12}$$

where ΔG_m^{fric} and ΔG_m^{strain} are the dissipation of Gibbs energy due to the interface friction and the transformation strain, respectively. ΔG_m^{chem} can

be expressed as:

$$\Delta G_m^{chem} = \sum_i^n x_i^{tr}\left(\mu_i^{\gamma/\alpha} - \mu_i^{\alpha}\right) \quad (13)$$

where i is the element in the steel, n is the number of elements, x_i^{tr} is the content of the element i transferred over the interface and it equals to x_i^{α} if diffusional flux in α_b matrix is neglected [54], μ_i^{α} and $\mu_i^{\gamma/\alpha}$ are the chemical potentials of element i at the interface in α_b and γ, respectively. It is worth mentioning that the diffusion of substitutional alloying elements inside the interface is not considered for the low-alloyed steels, since it is well established that substitutional alloying elements do not have sufficient time to segregate into the migrating interface during the fast lengthening process [47,55]. Contributions of substitutional alloying elements to the growth behavior of α_b were considered through their thermodynamic effects in Eq. (13). It has been suggested by Hillert [25] that the interface mobility for the lengthening process of α_b could be very high due to the similarity with the martensitic transformation. Thus, ΔG_m^{fric} can be neglected. Theoretical analyses [56,57] have shown that the transformation strain energy strongly depends on the volume fraction of α_b. When the volume fraction of α_b is not very large, the transformation strain energy is extremely small. For the sake of simplicity, ΔG_m^{strain} is neglected in the current case in which the α_b precipitates in an infinite γ, but the model can be used to make an estimate of the effect of transformation strain on transformation kinetics by bringing it explicitly into the governing equations (see Discussion section).

3.2. Model parameters

In the present model, there are two critical unknown parameters, $\sigma^{\alpha/\gamma}$ and D_C^{Intf}. As shown in Fig. 2a, a constant value of $\sigma^{\alpha/\gamma} = 0.23\,J/m^2$ was initially estimated by Hillert [25] while it was later optimized by Leach et al. [39] to be $0.10\,J/m^2$. According to the Gibbs absorption theory [58], carbon segregation into boundary would reduce the interfacial energy. Since the segregation tendency increases with decreasing temperature, smaller values of $\sigma^{\alpha/\gamma}$ are expected at low temperatures [59,60]. Making use of the fact that the ferrite/austenite interfacial energy at high temperatures has been estimated experimentally [28,61] and theoretically [62], the values of $\sigma^{\alpha/\gamma}$ at low temperatures can be linearly extrapolated from those at evaluated temperatures:

$$\sigma^{\alpha/\gamma} = -0.11 + 3.3\times10^{-4}T\ J/m^2 \quad (14)$$

where T is the numerical value (unitless) of absolute temperature. It is worth noting that the obtained values of $\sigma^{\alpha/\gamma}$ at low temperatures (<~773K) are quite comparable with those suggested by Quidort and Brechet [63] for the nucleation of α_b.

The dependence of carbon diffusivity on temperature and carbon content in γ has been established by Ågren [50]:

$$D_C^{\gamma} = 4.53\times10^{-7}\left[1 + y_C^{\gamma}(1-y_C^{\gamma})\frac{8339.9}{T}\right] \times\exp\left[-\left(\frac{1}{T} - 2.221\times10^{-4}\right)(17767 - 26436y_C^{\gamma})\right] m^2/s \quad (15)$$

where T is the numerical value (unitless) of absolute temperature and $y_C^{\gamma} = x_C^{\gamma}/(1-x_C^{\gamma})$ is the site fraction of carbon in γ. In contrast, the dependence of D_C^{Intf} on the temperature and composition is totally unknow. As shown in Fig. 2b, D_C^{Intf} is assumed to be $\sqrt{D_C^{\alpha}\cdot D_{C;0}^{\gamma}}$, where D_C^{α} is the diffusion coefficient of carbon in carbon supersaturated α used by Mujahid and Bhadeshia [64] and $D_{C;0}^{\gamma}$ is the diffusion coefficient of carbon in γ for zero carbon content (see Eq. (15)). Therefore, D_C^{Intf} is independent of the carbon content inside the interface, which can be calculated as:

$$D_C^{Intf} = 2.78\times10^{-6}\exp\left(-\frac{120.31kJ/mol}{RT}\right) m^2/s \quad (16)$$

The thickness of the α/γ interface 2δ is assumed to be 0.5 nm, which represents 2~3 atomic layers. The molar volume of the whole system is assumed to be constant and $V_m = 7\times10^{-6}m^3/mol$ was used. The thermodynamic parameters were evaluated using the TCFE7 database of Thermo-Calc software.

4. Results

4.1. Determination of lengthening rate and carbon content in bainitic ferrite

In the present model, all possible interfacial conditions that satisfies Eqs. (4) and (10)–(13) can be obtained by varying the choice of x_C^{α} and $x_C^{\gamma/\alpha}$. A flowchart describing the calculation procedure is given in Fig. 3. Fig. 4 shows the calculated dependence of the lengthening rate on carbon content in α_b for the MC steels at 723K (450℃). The upper limit for carbon content in α_b is much lower than the bulk carbon content, which indicates that a significant carbon redistribution is required for the growth of α_b. It is also observed that the lengthening rate would reach a maximum value as indicated by a solid square at a specific carbon content in α_b, which is very close to the upper limit for carbon content in α_b. According to the Zener's maximum growth rate hypothesis [65], the lengthening tip would spontaneously adjust its state until it has reached

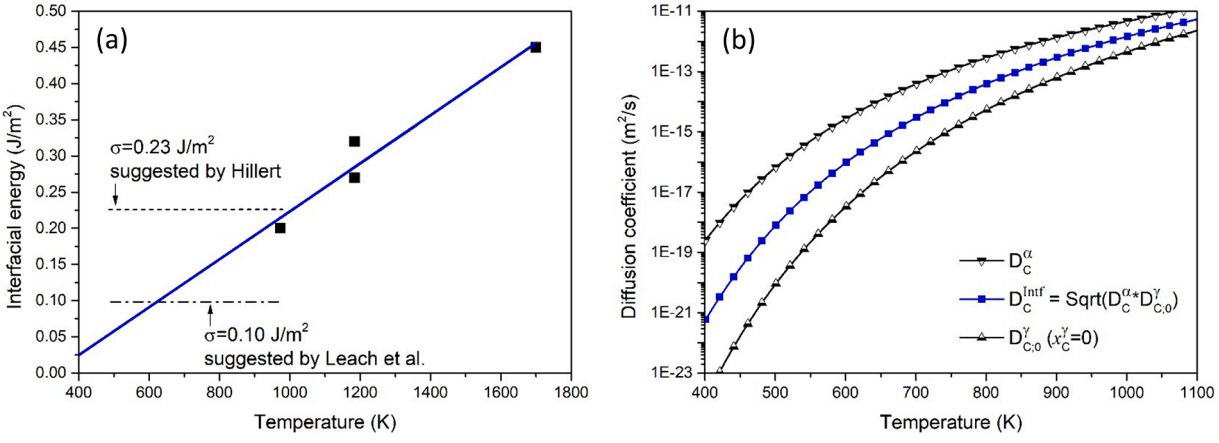

Fig. 2. The temperature dependence of (a) ferrite/austenite interfacial energy and (b) diffusion coefficient of carbon. The data points in (a) are obtained from Refs [28,61,62].

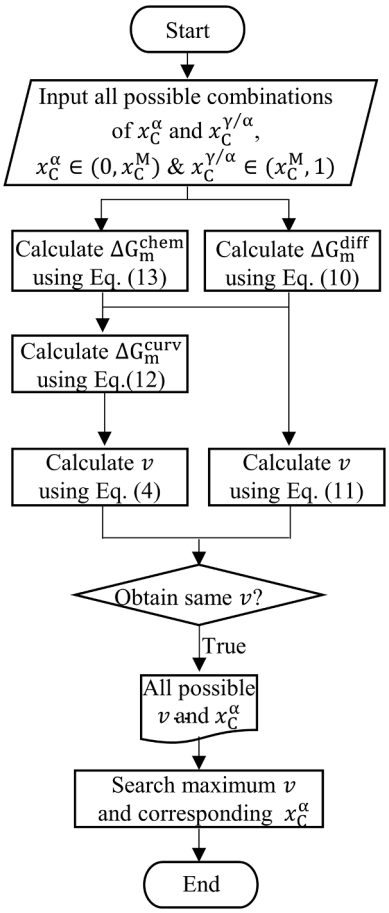

Fig. 3. Flowchart for the calculation procedure of the new model.

the maximum growth rate. Therefore, the maximum lengthening rate and its corresponding carbon content in α_b were chosen in the current model.

4.2. Applications to Fe-C steels

In order to develop a comprehensive understanding of the growth behavior of α_b, both the new model and the classical Z-H model were initially employed to predict the lengthening rate and carbon content in α_b for the MC, HC-1, and HC-2 steels, as shown in Fig. 5. Fig. 5a illustrates the lengthening rates for these three Fe-C steels predicted by the two models, along with a comparison to experimental data. It shows that at high temperatures the new model predictions are quite comparable with the Z-H model predictions. However, at low temperatures the lengthening rates predicted by the Z-H model are larger than those predicted by the new model and the discrepancies between them become more pronounced with decreasing temperature. It should be acknowledged that both models do not take into account the presence of carbide precipitation in bainite for the Fe-C steels. Consequently, this limitation may cause some discrepancies between the model predictions and the experimental measurements [29], with the measured lengthening rate necessarily being higher than the predicted value. Therefore, the new model shows a much better agreement with experiments than the Z-H model over a wide range of bulk carbon contents and transformation temperatures, which also indicates that carbide precipitation did not play a critical role during the lengthening of α_b.

Fig. 5b presents the carbon content in α_b for the three Fe-C steels predicted by the new model as well as the Z-H model. Additionally, the (para-)equilibrium carbon content in α_b between ferrite and austenite is included for comparison. As naturally expected, the carbon content in α_b calculated by the Z-H model is quite comparable with but slightly lower than the (para-)equilibrium level. Notably, the carbon content in α_b predicted by the new model remains lower than the (para-)equilibrium level at higher temperatures, e.g. above ~723K (450℃) for the MC steels. However, at lower temperatures, the carbon content in α_b surpasses the (para-)equilibrium level, and the disparities between them become significantly more pronounced with decreasing temperature. Generally, the dependence of carbon content in α_b on temperature predicted by the new model is opposite to the (para-)equilibrium and the Z-H model predictions. The new results clearly show that carbon supersaturated α_b could precipitate at low temperatures. However, when carbide precipitation takes place, it is challenging for the Fe-C steels to validate any model against experimental data on carbon supersaturation levels .

To illustrate the effects of bulk carbon content and transformation temperature on the formation of α_b, Fig. 5c show ΔG_m^{curv} and ΔG_m^{diff} as a function of transformation temperature for the MC, HC-1 and HC-2 steels. In three steels, ΔG_m^{curv} increases appreciably and then gradually reaches a constant value about 500 J/mol with decreasing temperature. ΔG_m^{diff} increases slightly and then increases linearly with decreasing temperature. At higher temperatures, e.g. above ~723K (450℃) for the MC steels, ΔG_m^{curv} is much larger than ΔG_m^{diff}, which indicates that the

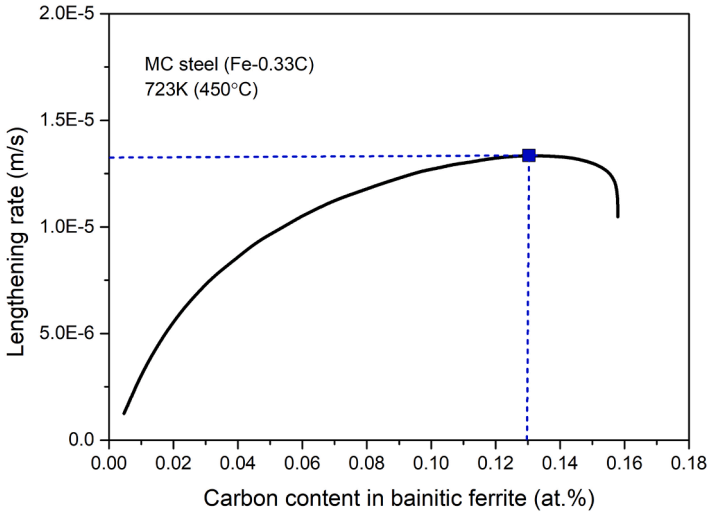

Fig. 4. The calculated dependence of lengthening rate on the carbon content in bainitic ferrite for the MC steels at 723K. The blue square refers to the obtained lengthening rate and carbon content in bainitic ferrite.

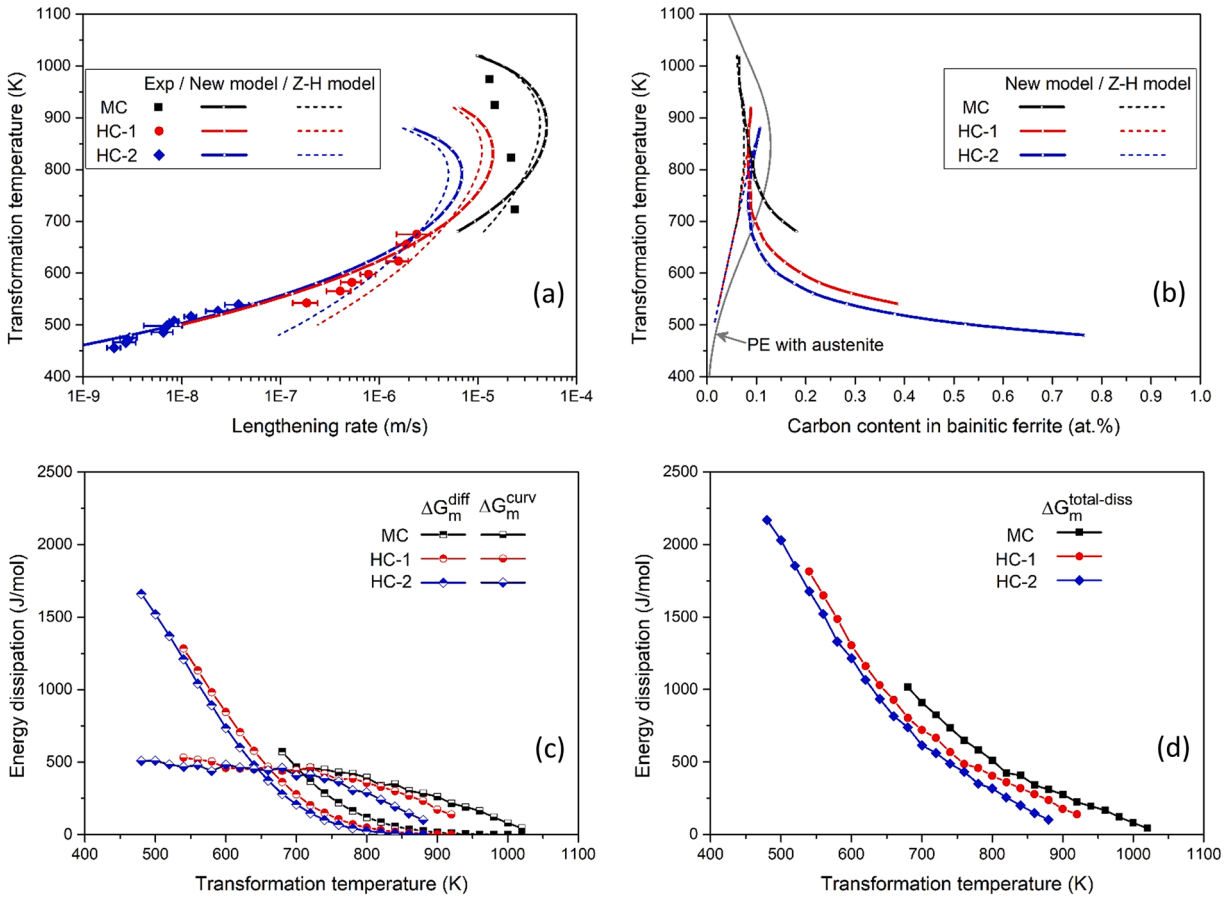

Fig. 5. The (a) lengthening rates and (b) carbon content in bainitic ferrite for the MC, HC-1 and HC-2 steels predicted by the new model as well as the classical Zener-Hillert model. The experimentally measured lengthening rates [28,30,31] and the (para-)equilibrium carbon content in bainitic ferrite between ferrite and austenite are shown in (a) and (b), respectively, for comparison. (c) ΔG_m^{curv}, ΔG_m^{diff} and (d) $\Delta G_m^{total-diss}$ as a function of transformation temperature for three steels.

capillarity effect due to the curvature would play a dominant role in the lengthening behavior of α_b. For this condition, the lengthening kinetics is mainly controlled by carbon diffusion ahead of the migrating interface, which is quite comparable with the description of the classical Z-H model. At lower temperatures, e.g. below ~723K (450℃) for the MC steels, ΔG_m^{diff} becomes larger than ΔG_m^{curv} and the discrepancies between them increase significantly with decreasing temperature. For this condition, carbon solute drag might play a more important role in the lengthening behavior of α_b. Thus, the lengthening behavior at low temperatures is mainly controlled by the carbon diffusion inside the interface itself. Fig. 5d further shows $\Delta G_m^{total-diss}$ as a function of transformation temperature for three Fe-C steels. It can be seen that $\Delta G_m^{total-diss}$ is strongly affected by the temperature as compared with the bulk carbon content. The predicted dependence of $\Delta G_m^{total-diss}$ on temperature is comparable with those estimated by Miyamoto et al. [3] and Leach et al. [40] for various steels, although it is assumed by them that carbon is in local equilibrium at the interface.

4.3. Applications to low alloyed steels

For the Fe-C steels, both the lengthening rate and carbon content in α_b could be affected by the presence of carbide precipitation, which effect is difficult to estimate and thus not considered in the new model. To avoid the possible interference of carbide precipitation on the model validation, the lengthening behavior of α_b in two medium carbon steels containing high Mn and Si contents was investigated using both the new model and the Z-H model. Fig. 6a shows the predicted lengthening rates of α_b for the MC-HSi-1 steels. The lengthening rates of individual α_b plates during linear cooling at approximately 380~370℃ and isothermal holding at 300℃ measured using in-situ TEM are shown for comparison. Although considerable scatter for the lengthening rate was observed in case of isothermal holding, most measurements fell within the range of $1 \times 10^{-7} \sim 1 \times 10^{-6}$m/s. It is clearly shown that the lengthening rates predicted by the new model, which are smaller than that predicted by the Z-H model, are in equally good agreement with experimental data both for the case of linear cooling and isothermal holding. Fig. 6b shows the comparison between the predicted and measured lengthening rates of α_b for the MC-HSi-2 steels. In addition to the lengthening rate of individual α_b plate during cooling, the average lengthening rates of various α_b plates with different nucleation sites during isothermal holding were also measured using in-situ CLSM. For the MC-HSi-2 steels, both the new model and the Z-H model show similar agreement with the experiments within the scatter of the experimental data. As shown in Figs. 5a and Fig. 6, the discrepancies between the new model predictions and experimental measurements on the lengthening rate for the Fe-C and low alloyed steels containing high Mn/Si contents are less than one order of magnitude.

To validate the prediction on carbon supersaturation in α_b, Fig. 7 shows the carbon content in α_b predicted by both the new model and the Z-H model, and the comparison against APT measurements for four low-alloyed steels, i.e. MC-LSi steel (Fig. 7a), MC-HSi-3 steel (Fig. 7b), HC-HSi-1 steel (Fig. 7c) and HC-HSi-2 steel (Fig. 7d). The paraequilibrium carbon content in α_b between ferrite and austenite is also shown for comparison. Clearly, both the paraequilibrium and the Z-H models fail to predict the dependence of carbon content in α_b on temperature for these four steels. In Fig. 7a, the carbon content in α_b predicted by the new model is lower than the paraequilibrium value at temperatures

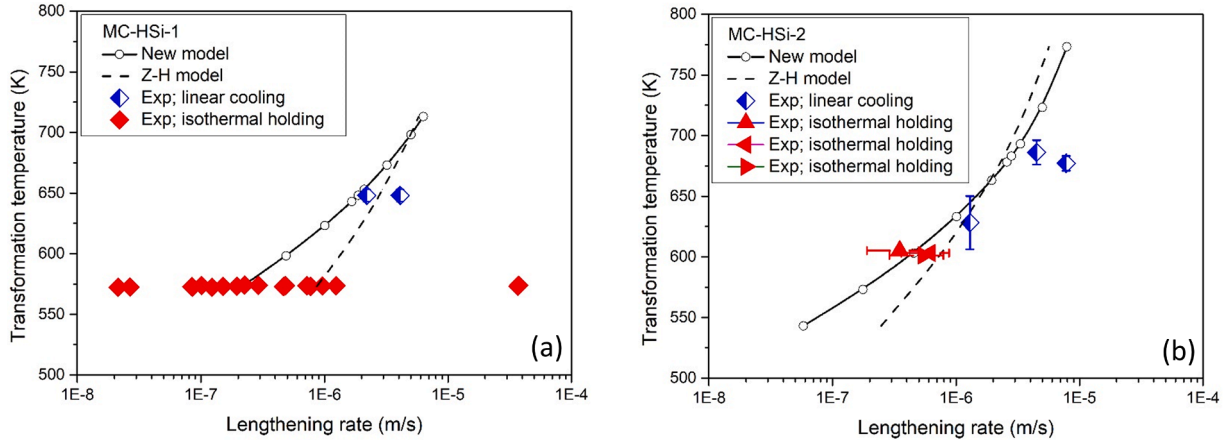

Fig. 6. Comparison between the predicted and measured lengthening rates for the (a) MC-HSi-1 and (b) MC-HSi-2 steels. The experimental data are obtained from Refs [32,34]. The red triangular points in (b) refer to the average lengthening rates of various individual bainitic ferrite plates with different nucleation sites, and other points in (a) and (b) refer to the lengthening rate of individual bainitic ferrite plate.

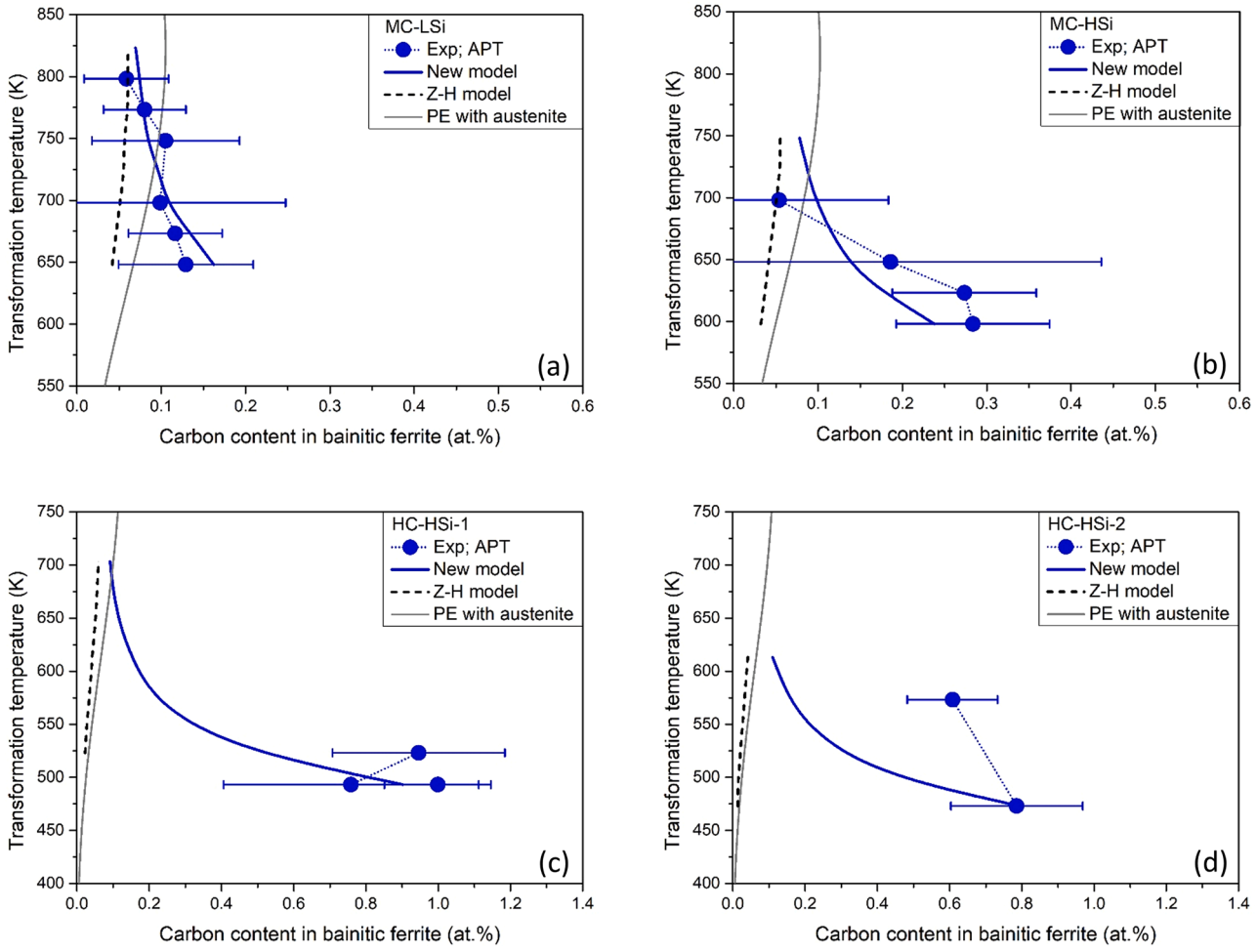

Fig. 7. Comparison between the predicted and measured carbon content in bainitic ferrite for the (a) MC-LSi, (b) MC-HSi-3, (c) HC-HSi-1 and (d) HC-HSi-2 steels. The experimental data are obtained from Refs [17,18]. The paraequilibrium carbon content in bainitic ferrite between ferrite and austenite is shown for comparison.

above ~723K (450℃) while it exceeds the paraequilibrium value at temperatures below ~723K (450℃). It is worth noting that cementite precipitation was observed experimentally in this steel due to the low Si content [17]. The good agreement between the new model predictions and experiments suggests that the effect of mild cementite precipitation on the carbon supersaturation in α_b is limited. This could be attributed to that cementite precipitates at the flat α/γ interface [66], instead of inside the α_b. By comparing Fig. 7a and b, it can be seen that the transformation temperature decreases with increasing Mn and Si contents. Accordingly, the degree of carbon supersaturation in α_b is predicted to further increase with decreasing temperature. These predictions are also in good agreement with experiments, as shown in Fig. 7b. When the

transformation temperature decreases significantly via enhancing the bulk carbon content from 0.3 wt.% (Fig. 7a and b) to 0.7 or 1.0 wt.% (see Fig. 7c or d), the predicted carbon content in α_b is more sensitive to temperature and increases significantly. It can be observed that the carbon content in α_b is extremely high and even up to ~0.9 at.% (~0.2 wt.%) for the high carbon steels, in case the transformation temperature is below ~523K (250℃). The strong influences of temperature and bulk carbon content on the carbon content in α_b for the low alloyed steels predicted by the new model are consistent with those for the Fe-C steels (see Fig. 5b).

The model was applied successfully to predict the growth behavior of α_b in multi-component steels. To show the effects of a single component Mn or Si on the growth behavior of α_b, the model was used to study the formation of α_b in the Fe-C-Mn/Si ternary alloys. Fig. 8a and b show the predicted lengthening rates and carbon content in α_b, respectively, for the Fe-0.3C and Fe-0.3C-3Mn/Si steels (all in wt.%). ΔG_m^{curv}, ΔG_m^{diff} (Fig. 8c) and $\Delta G_m^{total-diss}$ (Fig. 8d) as a function of transformation temperature for three steels are also given. The lengthening rates and carbon content in α_b are found to decrease with enhancing bulk Mn content, but are marginally affected by enhancing bulk Si content. The distinctive roles of Mn and Si in ΔG_m^{diff} and $\Delta G_m^{total-diss}$, i.e. ΔG_m^{chem}, are also observed. In contrast, ΔG_m^{curv} is found to be almost unaffected by Mn/Si addition.

5. Discussion

5.1. Effects of Mn and Si on the growth of bainitic ferrite

To elucidate why Mn but not Si shows a thermodynamic effect on the growth of α_b, the interfacial conditions, i.e. x_C^{α}, $x_C^{\gamma/\alpha}$ and $\Delta\mu_C = \mu_C^{\alpha} - \mu_C^{\gamma/\alpha}$, and the corresponding Gibbs energy curves of α and γ at 673K (400℃) for the Fe-0.3C and Fe-0.3C-3.0Mn/Si steels are plotted in Fig. 9. It is worth noting that a linear transformation of the Gibbs energy curves proposed by Gamsjäger [67] was adopted here, which does not alter the thermodynamics and thus allows for a better demonstration. In this treatment, the tangent at $x_C^{\gamma/\alpha}$ on the original Gibbs energy curve of γ is taken as the energy reference line, so that the interfacial conditions can be compared for three steels. It can be clearly seen from Fig. 9 that additions of Mn result in a reduction in x_C^{α} as well as $x_C^{\gamma/\alpha}$. Consequently, the difference in carbon chemical potential, i.e. $\mu_C^{\alpha} - \mu_C^{\gamma/\alpha}$ in Eq. (8), significantly decreases, indicating that the lengthening rate of α_b would be decelerated by additions of Mn. In contrast, since the addition of Si has almost no effect on the interfacial conditions, the lengthening rate of α_b is unaffected by Si additions.

The thermodynamic assumptions and predictions on the roles of Mn/Si made by the new model are indirectly supported by the WBs theory [8]. In this theory, Hillert et al. [8] also suggested that Mn and Si only affect the lengthening rate of α_b through their thermodynamic roles in α_b and γ. On this basis, it has been predicted and validated that Mn, but not Si, shows a thermodynamic effect on the kinetics of bainitic

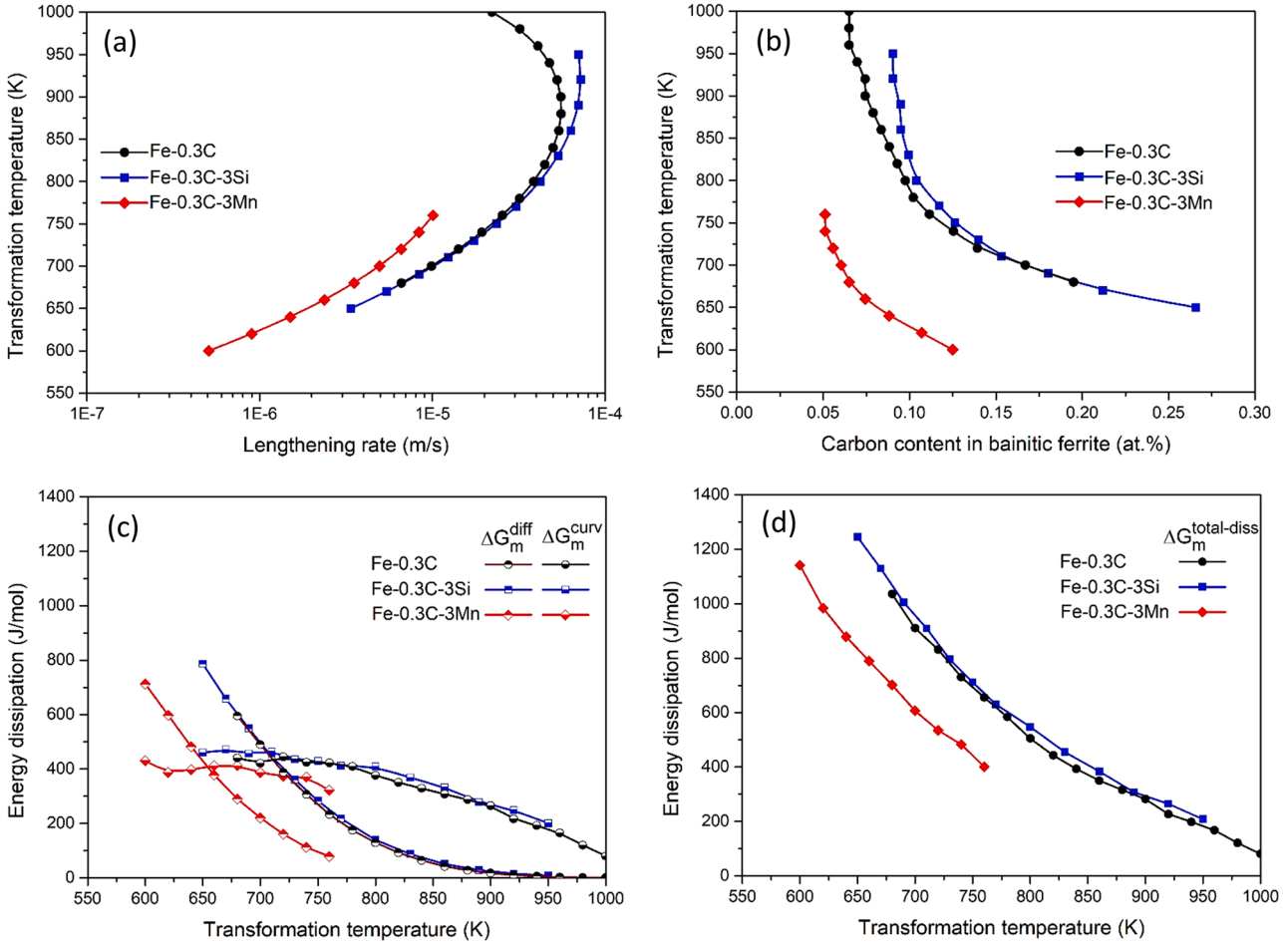

Fig. 8. The predicted (a) lengthening rates and (b) carbon content in bainitic ferrite for the Fe-0.3C and Fe-0.3C-3Mn/Si (all in wt.%) steels. (c) ΔG_m^{curv}, ΔG_m^{diff} and (d) $\Delta G_m^{total-diss}$ as a function of transformation temperature for three steels.

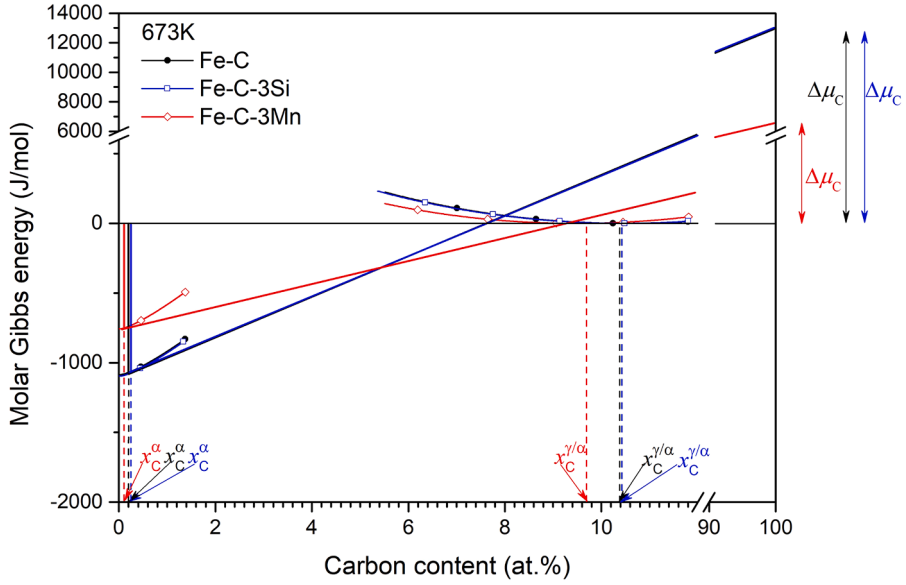

Fig. 9. The interfacial conditions and the corresponding Gibbs energy curves of α and γ for the Fe-0.3C and Fe-0.3C-3Mn/Si (all in wt.%) steels at 673K. Note that the Gibbs energy curves for the Fe-C-3Si systems almost coincide with those for the Fe-C systems. The vertical solid line at x_C^{α} represents $\Delta G_m^{total-diss}$, i.e. ΔG_m^{chem}.

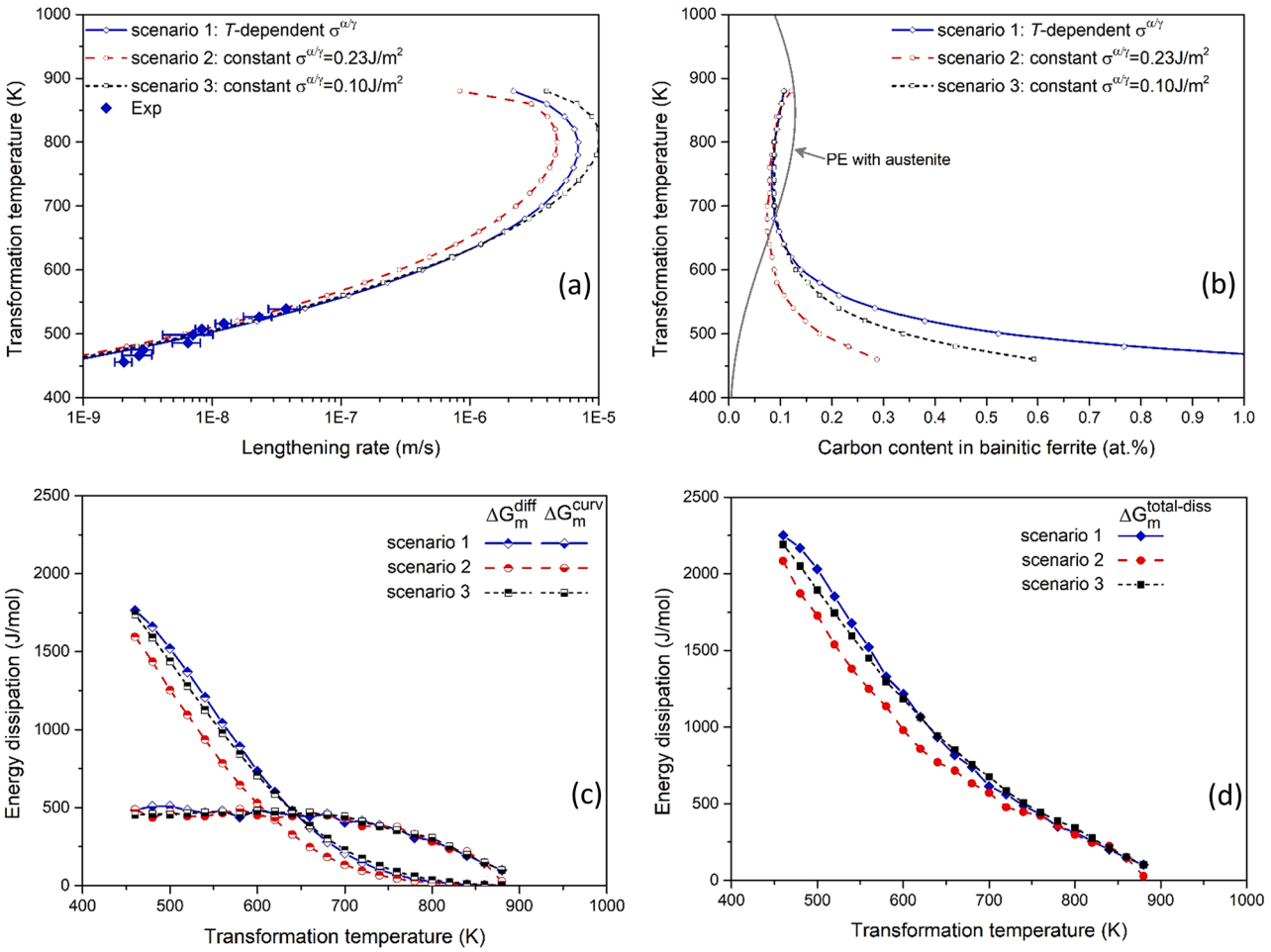

Fig. 10. The predicted (a) lengthening rates and (b) carbon content in bainitic ferrite for the HC-2 steels in three scenarios with different $\sigma^{\alpha/\gamma}$. (c) ΔG_m^{curv}, ΔG_m^{diff} and (d) $\Delta G_m^{total-diss}$ as a function of transformation temperature for three scenarios.

transformation and carbon enrichment in austenite [8,15].

5.2. Roles of $\sigma^{\alpha/\gamma}$ and D_C^{Intf} in the growth of bainitic ferrite

To show the effect of $\sigma^{\alpha/\gamma}$ on the growth of α_b, the lengthening rates (Fig. 10a) and carbon content in α_b (Fig. 10b) for the HC-2 steels were calculated in three scenarios. The first scenario corresponds to the new model predictions with a temperature-dependent $\sigma^{\alpha/\gamma}$. In the second and third scenarios, a constant $\sigma^{\alpha/\gamma}$ value of either 0.23J /m^2 [25] or 0.10J /m^2 [39] was assumed, respectively. Fig. 10a and b show that an increase in $\sigma^{\alpha/\gamma}$ slows down the lengthening rate at high temperatures and reduces the degree of carbon supersaturation in α_b at low temperatures. ΔG_m^{curv}, ΔG_m^{diff} (Fig. 10c) and $\Delta G_m^{total-diss}$ (Fig. 10d) as a function of transformation temperature are given for three scenarios. Fig. 10c and d demonstrate that an increase in $\sigma^{\alpha/\gamma}$ has a marginal effect on ΔG_m^{curv}, but results in a slight reduction in both ΔG_m^{diff} and $\Delta G_m^{total-diss}$.

As illustrated above, the choice of $\sigma^{\alpha/\gamma}$ mainly affects the degree of carbon supersaturation in α_b at low temperatures. The assumed dependence of interfacial energy on temperature for the α/γ interface (see Eq. (14)) is quite comparable with that for the grain boundary energy in various alloys [60]. Thus, similar to the grain boundary solute segregation effect [60], the weakening effect of temperature on $\sigma^{\alpha/\gamma}$ could be attributed to a stronger segregation tendency of carbon within the α/γ interface at lower temperatures. An APT analysis of a low alloyed Fe-C-Mn alloy held at 700°C did not show any carbon segregation within the α/γ interface [68], while a high degree of carbon segregation has been observed in a medium Mn steel during slow cooling at low temperatures [69]. Although the effect of solute segregation on $\sigma^{\alpha/\gamma}$ has rarely been reported, studies based on the Gibbs adsorption isotherm on other alloys suggested that solute segregation would lead to the reduction in the interphase boundary energy [70,71]. It is worth noting that, in this study, the carbon segregation behavior was not considered for simplicity. Further work should be done to consider the carbon segregation behavior and its effects on $\sigma^{\alpha/\gamma}$.

To show the effect of D_C^{Intf} on the growth of α_b, the lengthening rates (Fig. 11a) and carbon content in α_b (Fig. 11b) for the HC-2 steels were calculated in three scenarios. The first scenario corresponds to the new model predictions. In the second and third scenarios, D_C^{Intf} was enlarged 10 fold and assumed to be equal to D_C^{α} (=20~200D_C^{Intf} at low temperatures, see Fig. 2b), respectively. Fig. 11a and b show that the lengthening rate and carbon content in α_b are almost not affected by D_C^{Intf} at high temperatures. At low temperatures, the lengthening rate increases while carbon content in α_b decreases with increasing D_C^{Intf}. Notably, carbon supersaturation in α_b is almost absent when D_C^{Intf} is as large as D_C^{α}. ΔG_m^{curv}, ΔG_m^{diff} (Fig. 11c) and $\Delta G_m^{total-diss}$ (Fig. 11d) as a function of the transformation temperature are further plotted for three scenarios. Fig. 11c and d show that ΔG_m^{curv} is not affected by D_C^{Intf}, while both ΔG_m^{diff} and $\Delta G_m^{total-diss}$ significantly decrease as D_C^{Intf} increases. It is interesting to note that ΔG_m^{diff} is still remarkable at low temperatures in the third scenario, even though the carbon supersaturation in α_b is almost absent. Considering that extrapolating the Ågren equation from high temperatures may introduce uncertainties in $D_{C;eff}^{\gamma}$ at low temperatures, the

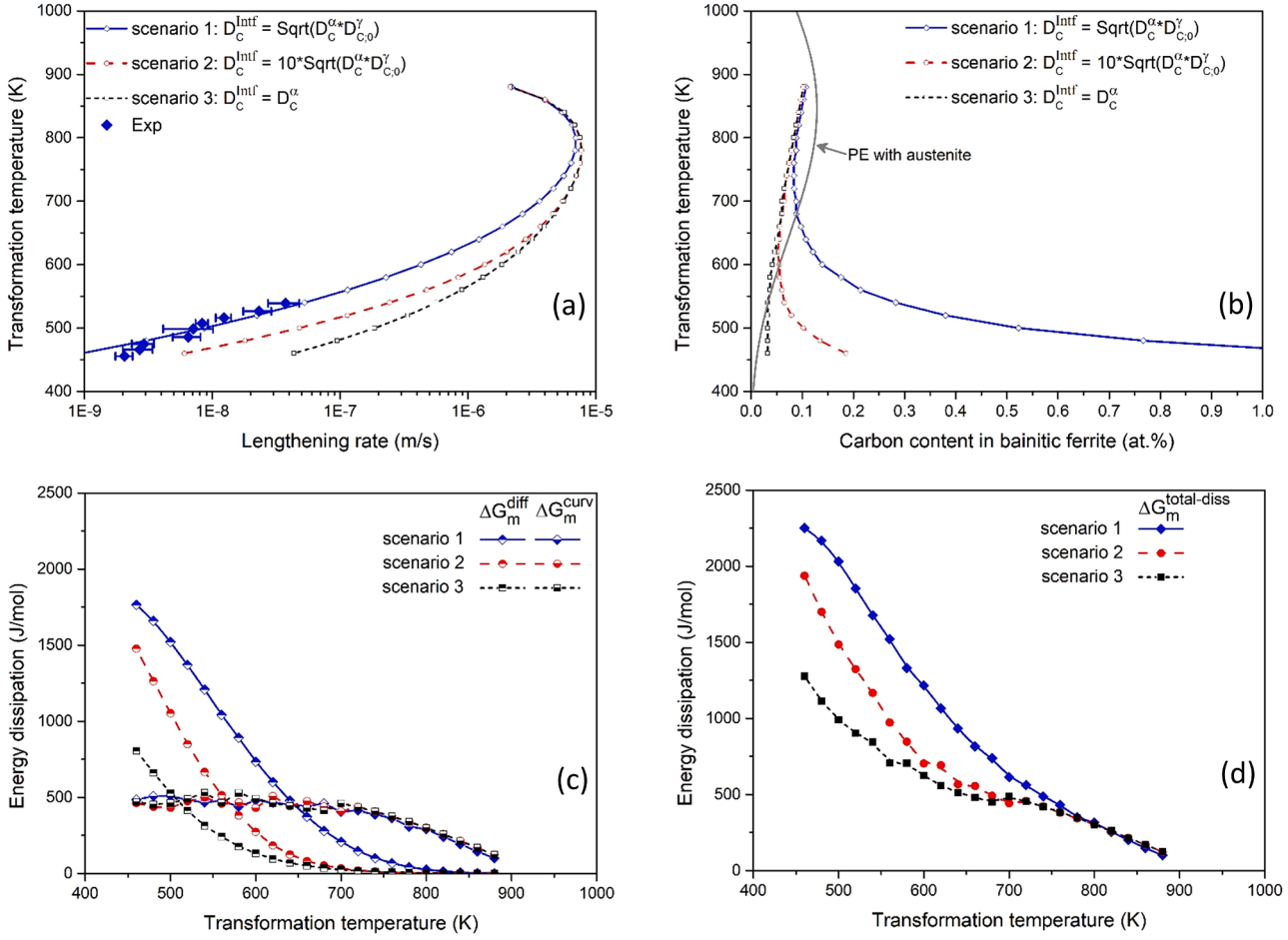

Fig. 11. The predicted (a) lengthening rates and (b) carbon content in bainitic ferrite for the HC-2 steels in three scenarios with different D_C^{Intf}. (c) ΔG_m^{curv}, ΔG_m^{diff} and (d) $\Delta G_m^{total-diss}$ as a function of transformation temperature for three scenarios.

effects of $D^{\gamma}_{C;eff}$ on the lengthening behavior of α_b were discussed in **Supplementary materials**.

The value of D^{Intf}_{C} holds significant importance in determining the lengthening rate and plays a crucial role in understanding the 'carbon supersaturation in α_b' phenomenon at low temperatures. The dependence of D^{Intf}_{C} on temperature and composition has less been investigated, since it is usually regarded that the diffusivity of carbon inside the interphase (or grain) boundary is large. Yet, recent findings from molecular dynamics simulations and experiments [72,73] have challenged this assumption by revealing that the diffusivity of carbon inside the ferrite grain boundary is lower than that in the bulk. Teus et al. [72] attributed the retardation effect to the drastic decrease or the disappearance of the elastic term in the chemical potential gradient due to the capture by grain boundary. Considering the more complex structure of an interphase boundary (α/γ boundary) compared to that of a grain boundary, it is reasonable to expect that the diffusion process of carbon inside the α/γ boundary will be strongly influenced by the intricate interaction between carbon and the interface.

5.3. Effect of transformation strain energy

In sections above, the Gibbs energy dissipated by transformation strain ΔG^{strain}_{m} was neglected. It is usually argued that the transformation strain play an important role in the growth of α_b, particularly at low temperatures. To explore the influences of transformation strain on the growth behavior of α_b, ΔG^{strain}_{m} in Eq. (12) was estimated using the method proposed by Benrabah et al. [12]. More details about the calculation can be found in **Supplementary materials**. Fig. 12a and b show the lengthening rates and carbon content in α_b, respectively, for the HC-2 steels predicted with and without considering ΔG^{strain}_{m}. In Fig. 12a, the predicted lengthening rate is retarded by the transformation strain at higher temperatures while it is marginally affected at lower temperatures. To better understand these results, ΔG^{strain}_{m}, ΔG^{curv}_{m}, ΔG^{diff}_{m} and $\Delta G^{total-diss}_{m}$ as a function of transformation temperature are shown in Fig. 13a. It can be seen that ΔG^{diff}_{m} is negligible due to the absence of carbon supersaturation in α_b at high temperatures. However, ΔG^{strain}_{m} is quite comparable with ΔG^{curv}_{m} and thus makes a great contribution to $\Delta G^{total-diss}_{m}$. As a result, the lengthening rate at high temperatures is retarded by taking ΔG^{strain}_{m} into account. In contrast, ΔG^{diff}_{m} is very large and much higher than ΔG^{strain}_{m} at low temperatures. ΔG^{strain}_{m} accounts for a small proportion in $\Delta G^{total-diss}_{m}$ and thus has a limited effect on the lengthening rate at low temperatures. Fig. 13a also shows that ΔG^{strain}_{m} gradually increases from ~150J/mol to ~400J/mol with decreasing temperature. ΔG^{strain}_{m} at low temperatures is quite comparable with the strain energy used for displacive α (with respect T_0 theory) [1,74], while ΔG^{strain}_{m} at high temperatures is much higher than the experimentally estimated value of ~20J/mol [75]. This could be attributed to that the parameters for the calculation of ΔG^{strain}_{m} were measured at low transformation temperatures, which are not applicable for the case of high temperatures. Therefore, the retardation effect of ΔG^{strain}_{m} on the lengthening rate at high temperatures could be overestimated. In Fig. 12b, the degree of carbon supersaturation in α_b is predicted to decrease by taking ΔG^{strain}_{m} into account, especially at low temperatures. To illustrate this result, Fig. 13b shows the energy dissipation associated with the carbon content in α_b for the HC-2 steel at 538K (265℃) predicted with and without considering the transformation strain. A linear transformation of the Gibbs energy curves used in Fig. 9 was adopted here. It can be seen that, when the additional energy dissipation due to the transformation strain is considered, more chemical driving force is required to balance the increased dissipation of Gibbs energy. Thus, the carbon content in α_b would shift to the left, which reduces the degree of carbon supersaturation in α_b.

Taking both the carbon solute drag effect and the transformation strain into account, the new model demonstrates its capability to correctly predict the lengthening rate and qualitatively interpret the phenomenon of carbon supersaturation in α_b. Interestingly, it appears that, when compared to the transformation strain, the carbon solute drag effect plays a more significant role in influencing the growth behavior of α_b, particularly at low temperatures.

6. Conclusions

A thermo-kinetic model based on the Zener-Hillert theory and the Gibbs energy balance concept was developed to investigate the growth mechanism of bainitic ferrite. The key feature of the model is the incorporation of the effect of the temperature dependent carbon diffusion inside the migrating interface. The new model was applied to predict the influences of temperature and composition on the lengthening rate and carbon content in bainitic ferrite for nine Fe-C and low alloyed steels. The model predictions were compared with experimental data published in the literature and the agreement was found to be excellent and much better than that for the classical Zener-Hillert model. The main conclusions are summarized as follows:

1. The lengthening rate of bainitic ferrite at high temperatures is dominated by carbon diffusion ahead of the migrating interface, which is comparable with the classical Zener-Hillert model predictions. In contrast, the lengthening rate of bainitic ferrite at low temperatures is mainly controlled by carbon diffusion inside the migrating interface, which indicates that carbon solute drag effect plays a significant role.

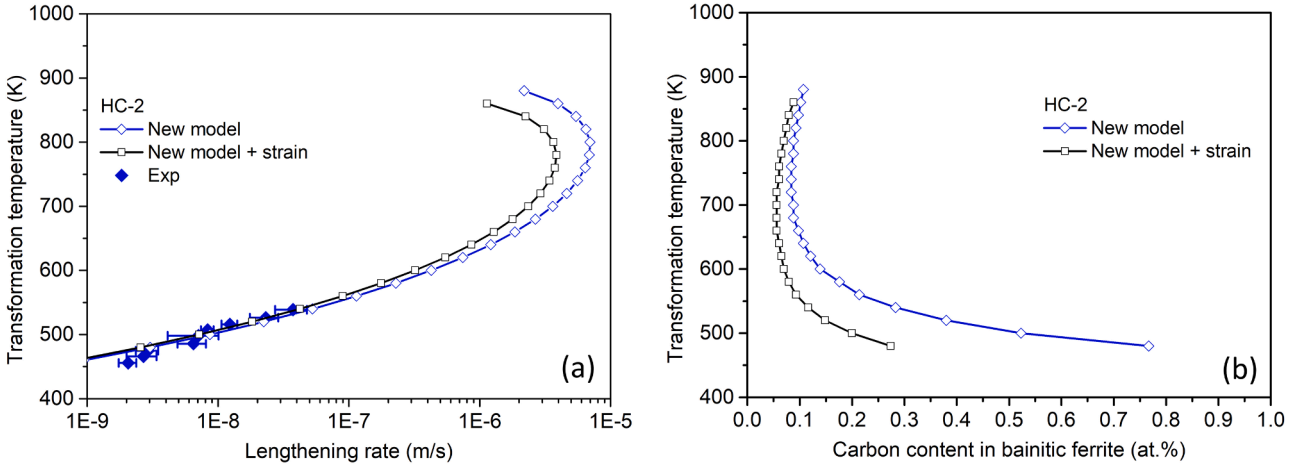

Fig. 12. The (a) lengthening rates and (b) carbon content in bainitic ferrite for the HC-2 steels predicted with and without considering the transformation strain.

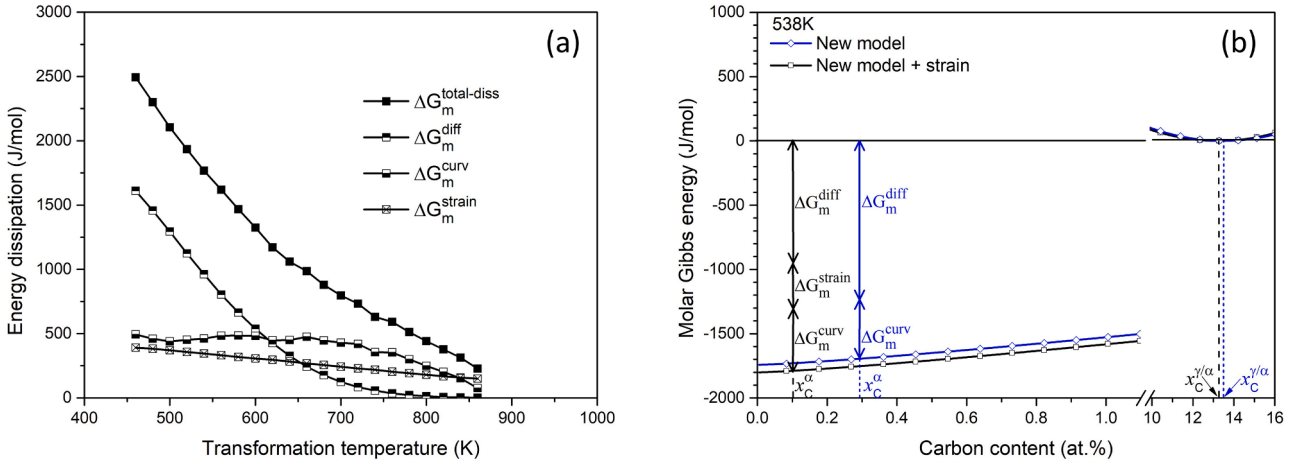

Fig. 13. (a) ΔG_m^{strain}, ΔG_m^{curv}, ΔG_m^{diff} and $\Delta G_m^{total-diss}$ as a function of transformation temperature for the HC-2 steels predicted with considering the transformation strain. (b) The Gibbs energy dissipation associated with carbon content in bainitic ferrite for the HC-2 steels at 538K predicted with and without considering the transformation strain.

2. The degree of carbon supersaturation in bainitic ferrite strongly depends on the transformation temperature. Significant supersaturation of carbon in bainitic ferrite at low temperatures leads to remarkable carbon solute drag effect on the lengthening rate of bainitic ferrite.

3. At low temperatures the lengthening rate of bainitic ferrite is marginally affected by the transformation strain but the degree of carbon supersaturation in bainitic ferrite decreases due to this strain.

Declaration of competing interest

The authors declare that they have no known competing financial interests or personal relationships that could have appeared to influence the work reported in this paper.

Acknowledgements

he authors acknowledge financial support from the National Key R&D Program of China (2023YFB3711700 and 2021YFB2402101), the Natural Science Basic Research Program of Shaanxi (2024JC-YBQN-0578), the Fundamental Research Funds for the Central Universities (xzy012023067) and ShaanXi Province Innovation Team Project (2024RS-CXTD-58).

Supplementary materials

Supplementary material associated with this article can be found, in the online version, at doi:10.1016/j.actamat.2024.119791.

References

[1] H.K.D.H. Bhadeshia, Bainite in Steels: Theory and Practice, Maney Publishing, 2015.
[2] Z. Dai, H. Chen, R. Ding, Q. Lu, C. Zhang, Z. Yang, S. van der Zwaag, Fundamentals and application of solid-state phase transformations for advanced high strength steels containing metastable retained austenite, Mater. Sci. Eng. R 143 (2021) 100590.
[3] G. Miyamoto, T. Furuhara, Interaction of alloying elements with migrating ferrite/austenite interface, Isij Int 60 (12) (2020) 2942–2953.
[4] M. Militzer, C. Hutchinson, H. Zurob, G. Miyamoto, Modelling of the diffusional austenite-ferrite transformation, Int. Mater. Rev. (2022) 1–30.
[5] L.C.D. Fielding, The bainite controversy, Mater. Sci. Technol. 29 (4) (2013) 383–399.
[6] W. Wei, P. Retzl, E. Kozeschnik, P.K. Erwin, A semi-physical α-β model on bainite transformation kinetics and carbon partitioning, Acta Mater 207 (2021) 116701.
[7] Y. Zhang, Y. He, Y. Zhang, S. Song, F. Liu, Bainitic transformation and generalized stability, Scr. Mater. 227 (2023) 115311.
[8] M. Hillert, L. Hoglund, J. Ågren, Role of carbon and alloying elements in the formation of Bainitic Ferrite, Metall. Mater. Trans. A 35A (2004) 3693–3700.
[9] A. Borgenstam, M. Hillert, J. Agren, Metallographic evidence of carbon diffusion in the growth of bainite, Acta Mater 57 (11) (2009) 3242–3252.
[10] H. Chen, K. Zhu, L. Zhao, S. van der Zwaag, Analysis of transformation stasis during the isothermal bainitic ferrite formation in Fe–C–Mn and Fe–C–Mn–Si alloys, Acta Mater 61 (14) (2013) 5458–5468.
[11] W.W. Sun, H.S. Zurob, C.R. Hutchinson, Coupled solute drag and transformation stasis during ferrite formation in Fe-C-Mn-Mo, Acta Mater 139 (2017) 62–74.
[12] I.E. Benrabah, Y. Brechet, G. Purdy, C. Hutchinson, H. Zurob, On the origin of the barrier in the bainite phase transformation, Scr. Mater. 223 (2023) 115076.
[13] Z.Q. Liu, G. Miyamoto, Z.G. Yang, T. Furuhara, Direct measurement of carbon enrichment during austenite to ferrite transformation in hypoeutectoid Fe–2Mn–C alloys, Acta Mater 61 (8) (2013) 3120–3129.
[14] Y. Xia, G. Miyamoto, Z.G. Yang, C. Zhang, T. Furuhara, Direct measurement of carbon enrichment in the incomplete bainite transformation in Mo added low carbon steels, Acta Mater 91 (2015) 10–18.
[15] H.D. Wu, G. Miyamoto, Z.G. Yang, C. Zhang, H. Chen, T. Furuhara, Incomplete bainite transformation in Fe-Si-C alloys, Acta Mater 133 (2017) 1–9.
[16] G. Miyamoto, K. Yokoyama, T. Furuhara, Quantitative analysis of Mo solute drag effect on ferrite and bainite transformations in Fe-0.4C-0.5Mo alloy, Acta Mater 177 (2019) 187–197.
[17] F.G. Caballero, M.K. Miller, C. Garcia-Mateo, J. Cornide, M.J. Santofimia, Temperature dependence of carbon supersaturation of ferrite in bainitic steels, Scr. Mater. 67 (10) (2012) 846–849.
[18] C. Garcia-Mateo, J.A. Jimenez, H.W. Yen, M.K. Miller, L. Morales-Rivas, M. Kuntz, S.P. Ringer, J.R. Yang, F.G. Caballero, Low temperature bainitic ferrite: Evidence of carbon super-saturation and tetragonality, Acta Mater 91 (2015) 162–173.
[19] E.V. Pereloma, Critical assessment 20: on carbon excess in bainitic ferrite, Mater. Sci. Technol. 32 (2) (2016) 99–103.
[20] S.H. Kim, J.H. Kim, K.S. Park, Y.R. Im, J.H. Lee, D.W. Suh, J.S. Lee, Analysis of transformation stasis by the Gibbs energy balance (GEB) approach modified to consider carbon redistribution into remaining austenite, Calphad 70 (2020) 101804.
[21] R. Ranjan, S.B. Singh, Isothermal bainite transformation in low-alloy steels: Mechanism of transformation, Acta Mater 202 (2021) 302–316.
[22] I. Pushkareva, J. Macchi, B. Shalchi-Amirkhiz, F. Fazeli, G. Geandier, F. Danoix, J. D.C. Teixeira, S.Y.P. Allain, C. Scott, A study of the carbon distribution in bainitic ferrite, Scr. Mater. 224 (2023) 115140.
[23] J.B. Seol, D. Raabe, P.P. Choi, Y.R. Im, C.G. Park, Atomic scale effects of alloying, partitioning, solute drag and austempering on the mechanical properties of high-carbon bainitic–austenitic TRIP steels, Acta Mater 60 (17) (2012) 6183–6199.
[24] S. Lin, A. Borgenstam, A. Stark, P. Hedström, Effect of Si on bainitic transformation kinetics in steels explained by carbon partitioning, carbide formation, dislocation densities, and thermodynamic conditions, Mater. Charact. 185 (2022) 111774.
[25] M. Hillert, The growth of ferrite, bainite and martensite, Internal Report of the Swedish Institute for Metal Research, Stockholm, Sweden, 1960.
[26] M. Hillert, Diffusion in Growth of Bainite, Metall. Mater. Trans. A 25A (1994) 1957–1966.
[27] M. Hillert, L. Höglund, J. Ågren, Diffusion-controlled lengthening of Widmanstätten plates, Acta Mater 51 (7) (2003) 2089–2095.
[28] E.P. Simonen, H.I. Aaronson, R. Trivedi, Lengthening kinetics of ferrite and bainite sideplates, Metall. Trans. 4 (5) (1973) 1239–1245.
[29] D. Quidort, Y.J.M. Brechet, Isothermal growth kinetics of bainite in 0.5% C steels, Acta Mater 49 (20) (2001) 4161–4170.
[30] G.R. Speich, M. Cohen, The growth rate of bainite, Trans. AIME 218 (1960) 1050–1059.
[31] M.J. Hawkins, J. Barford, Experimental kinetics of bainite formation, J. Iron Steel Inst. 210 (2) (1972) 97–105.

[32] Z.w. Hu, G. Xu, H.j. Hu, L. Wang, Z.l. Xue, In situ measured growth rates of bainite plates in an Fe-C-Mn-Si superbainitic steel, Int. J. Miner. Metall. 21 (4) (2014) 371–378.
[33] H. Hu, B. Imed-Eddine, G. Xu, J. Tian, M. Zhou, Y. Bréchet, H.S. Zurob, Effect of temperature, carbon content and crystallography on the lengthening kinetics of bainitic ferrite laths, Mater. Charact. 187 (2022) 111860.
[34] J. Nutter, J. Qi, H. Farahani, W.M. Rainforth, S. van der Zwaag, In situ TEM observations of the growth of bainitic ferrite in an Fe-0.3C-3Mn-1.5Si-0.15Mo steel, Acta Mater. 252 (2023) 118924.
[35] M. Hillert, The Nature of Bainite, Isij Int 35 (9) (1995) 1134–1140.
[36] L. Kaufman, S.V. Radcliffe, M. Cohen, Decomposition of Austenite by Diffusional Processes, Inderscience Publishers, New York, 1963, pp. 313–352.
[37] L. Leach, M. Hillert, A. Borgenstam, Modeling C-Curves for the Growth Rate of Widmanstätten and Bainitic Ferrite in Fe-C Alloys, Metall. Mater. Trans. A 47 (1) (2015) 19–25.
[38] S. Sainis, H. Farahani, E. Gamsjäger, S. van der Zwaag, An in-situ LSCM Study on Bainite Formation in a Fe-0.2C-1.5Mn-2.0Cr Alloy, Metals 8 (7) (2018) 498.
[39] L. Leach, J. Ågren, L. Höglund, A. Borgenstam, Diffusion-controlled lengthening rates of Bainitic Ferrite a part of the steel genome, Metall. Mater. Trans. A 50 (2019) 2613–2618.
[40] L. Leach, P. Kolmskog, L. Hoglund, M. Hillert, A. Borgenstam, Critical Driving Forces for Formation of Bainite, Metall. Mater. Trans. A 49 (10) (2018) 4509–4520.
[41] M. Goune, F. Danoix, J. Agren, Y. Brechet, C.R. Hutchinson, M. Militzer, G. Purdy, S. van der Zwaag, H. Zurob, Overview of the current issues in austenite to ferrite transformation and the role of migrating interfaces therein for low alloyed steels, Mater. Sci. Eng. R 92 (2015) 1–38.
[42] M. Hillert, Solute drag, solute trapping and diffusional dissipation of Gibbs energy, Acta Mater 47 (18) (1999) 4481–4505.
[43] M. Hillert, Solute drag in grain boundary migration and phase transformations, Acta Mater 52 (18) (2004) 5289–5293.
[44] J. Ågren, A simplified treatment of the transition from diffusion controlled to diffusion-less growth, Acta Metall 37 (1) (1989) 181–189.
[45] Z.K. Liu, Theoretic calculation of ferrite growth in supersaturated austenite in Fe-C alloy, Acta Mater 44 (9) (1996) 3855–3867.
[46] M. Suehiro, Z.K. Liu, J. Ågren, Effect of niobium on massive transformation in ultra low carbon steels: a solute drag treatment, Acta Mater 44 (10) (1996) 4241–4251.
[47] Z.K. Liu, The transformation phenomenon in Fe-Mo-C alloys: A solute drag approach, Metall. Mater. Trans. A 28 (8) (1997) 1625–1631.
[48] S.M.C. van Bohemen, Bainite and martensite start temperature calculated with exponential carbon dependence, Mater. Sci. Technol. 28 (4) (2012) 487–495.
[49] M. Hillert, The role of interfacial energy during solid state phase transformations, Jernkont. Ann. 141 (1957) 757–789.
[50] J. Ågren, A revised expression for the diffusivity of carbon in binary Fe-C austenite, Scr. Metall. 20 (11) (1986) 1507–1510.
[51] R. Trivedi, G.M. Pound, Effect of concentration-dependent diffusion coefficient on the migration of interphase boundaries, J. Appl. Phys. 38 (9) (1967) 3569–3576.
[52] G.R. Purdy, Y.J.M. Brechet, A solute drag treatment of the effects of alloying elements on the rate of the proeutectoid ferrite transformation in steels, Acta Metall. Mater. 43 (10) (1995) 3763–3774.
[53] E. Gamsjäger, M. Rettenmayr, The kinetics of diffusive phase transformations in the light of trans-interface diffusion, Philos. Mag. 95 (26) (2015) 2851–2865.
[54] M. Hillert, J. Odqvist, J. Ågren, Interface conditions during diffusion-controlled phase transformations, Scr. Mater. 50 (4) (2004) 547–550.
[55] H. Chen, Z. Yang, C. Zhang, K. Zhu, S. van der Zwaag, On the transition between grain boundary ferrite and bainitic ferrite in Fe–C–Mo and Fe–C–Mn alloys: The bay formation explained, Acta Mater 104 (2016) 62–71.
[56] D. Quidort, O. Bouaziz, The Bainite transformation stage in the processing of trip-aided sheet steels, Can. Metall. Quart 43 (1) (2013) 25–34.
[57] S.M.C. van Bohemen, Bainite growth retardation due to mechanical stabilisation of austenite, Materialia 7 (2019) 100384.
[58] J.W. Gibbs, The Collected Works of J. Willard Gibbs, Yale University Press, 1948.
[59] N.A. Gjostein, H.A. Domian, H.I. Aaronson, E. Eichen, Relative interfacial energies in Fe-C alloys, Acta Metall 14 (12) (1966) 1637–1644.
[60] D. Gupta, Diffusion, solute segregations and interfacial energies in some material: an overview, Interface Sci 11 (1) (2003) 7–20.
[61] H. Yin, T. Emi, H. Shibata, Determination of free energy of δ-ferrite/γ-austenite interphase boundary of low carbon steels by in-situ observation, Isij Int 38 (8) (1998) 794–801.
[62] T. Nagano, M. Enomoto, Calculation of the interfacial energies between α and γ iron and equilibrium particle shape, Metall. Mater. Trans. A 37 (3) (2006) 929–937.
[63] D. Quidort, Y.J.M. Brechet, A Model of Isothermal and Non Isothermal Transformation Kinetics of Bainite in 0.5% C Steels, Isij Int 42 (9) (2002) 1010–1017.
[64] S.A. Mujihid, H.K.D.H. Bhadeshia, Partitioning of carbon from supersaturated ferrite plates, Acta Metall. Mater. 40 (2) (1992) 389–396.
[65] C. Zener, Kinetics of the decomposition of austenite, Trans. AIME 167 (1946) 550–590.
[66] G. Spanos, H.S. Fang, H.I. Aaronson, A mechanism for the formation of lower bainite, Metall. Trans. A 21 (6) (1990) 1381–1390.
[67] E. Gamsjäger, A note on the contact conditions at migrating interfaces, Acta Mater 55 (14) (2007) 4823–4833.
[68] O. Thuillier, F. Danoix, M. Goune, D. Blavette, Atom probe tomography of the austenite–ferrite interphase boundary composition in a model alloy Fe–C–Mn, Scr. Mater. 55 (11) (2006) 1071–1074.
[69] Y. Ma, B. Sun, A. Schökel, W. Song, D. Ponge, D. Raabe, W. Bleck, Phase boundary segregation-induced strengthening and discontinuous yielding in ultrafine-grained duplex medium-Mn steels, Acta Mater 200 (2020) 389–403.
[70] I. Blum, S.I. Baik, M.G. Kanatzidis, D.N. Seidman, An integral method for the calculation of the reduction in interfacial free energy due to interfacial segregation, arXiv e-prints (2020) arXiv:2003.01246.
[71] Y. Huang, Z. Mao, R.D. Noebe, D.N. Seidman, The effects of refractory elements on Ni-excesses and Ni-depletions at γ(f.c.c.)/γ′(L12) interfaces in model Ni-based superalloys: Atom-probe tomographic experiments and first-principles calculations, Acta Mater 121 (2016) 288–298.
[72] S.M. Teus, V.F. Mazanko, J.M. Olive, V.G. Gavriljuk, Grain boundary migration of substitutional and interstitial atoms in α-iron, Acta Mater 69 (2014) 105–113.
[73] O.A. Restrepo, N. Mousseau, M. Trochet, F. El-Mellouhi, O. Bouhali, C.S. Becquart, Carbon diffusion paths and segregation at high-angle tilt grain boundaries inα-Fe studied by using a kinetic activation-relation technique, Phys. Rev. B 97 (5) (2018) 054309.
[74] L.K. Huang, F. Liu, M.X. Huang, Accelerating bainite transformation by concurrent pearlite formation in a medium Mn steel: Experiments and modelling, J. Mater. Sci. Technol. 176 (2024) 211–223.
[75] H. Dong, Y. Zhang, G. Miyamoto, H. Chen, Z. Yang, T. Furuhara, A comparative study on intrinsic mobility of incoherent and semicoherent interfaces during the austenite to ferrite transformation, Scr. Mater. 188 (2020) 59–63.